Research on Suppression of Airflow Secondary Noise in a Muffler Based on Large Eddy Simulation

Bo Zhao and He Li

School of Mechanical Engineering and Automation, Northeastern University, Shenyang 110819, China.
E-mail: hli@mail.neu.edu.cn

(Received 3 May 2022; accepted 11 October 2022)

Based on the Large Eddy Simulation (LES), the problem of the performance of a muffler being weakened by the airflow secondary noise in the expansion chamber was analyzed. Based on the different relative positions of the inlet and outlet, a single-chamber muffler is divided into four structures and a numerical simulation model of the flow field is developed. The LES was used to analyze the flow field and secondary noise in the expansion chamber. First, the LES is used to calculate the unsteady flow in the expansion chamber to obtain the turbulent intensity and the pressure pulsation distribution of the flow in the muffler chamber. Subsequently, a simulation model of the acoustic field was built separately to obtain the secondary noise distribution of the flow in the muffler by computing the flow field information. It is shown that the secondary noise properties in the muffler are related to its geometrical configuration. The turbulence intensity of the flow field in the chamber can be reduced by changing the airflow pattern in the chamber, to weaken the intensity of the airflow secondary noise. Finally, a structural modification of the two-chamber muffler was performed based on the findings of the study, and the improved muffler performance was evaluated through numerical simulations and field tests. Experimental results show that the improved muffler has better acoustic properties and increases the noise reduction capacity by about 18 percent. It further confirms that the intensity of secondary noise can be substantially suppressed by changing the internal structure of the muffler, which opens up new ideas for the future design and modification of exhaust mufflers.

1. INTRODUCTION

In the 21st century, noise has become another major threat to human public health. Installing exhaust mufflers is one of the most widely used measures to effectively reduce exhaust noise from machinery and equipment.[1–3]

The principle of the exhaust muffler is to reduce the sound energy output by reflecting or interfering with sound waves in the pipe and the resonant chamber. The calculation methods of the muffler performance mainly include the analytical method and the numerical method. The analytical method has high computational efficiency but is inaccurate enough when faced with complex structures. The numerical methods can be divided into frequency-domain simulation and time-domain simulation. At present, the frequency-domain calculation has been extensively used.

There are two calculation methods in the frequency domain, the finite element method (FEM), and the boundary element method (BEM). They are both based on the linearity hypothesis to solve the acoustic equations to obtain the required parameters. In summary, the FEM and BEM currently calculate the acoustic performance of mufflers by solving linearized wave equations but are ineffective in solving various nonlinear parameters. The computational fluid dynamics (CFD) method uses the Navier-Stokes equations as the main governing equations. It has significant advantages over the FEM and BEM in dealing with non-ideal fluid media.[4–7]

British meteorologist, L. F. Richardson, used the finite difference method to solve the Laplace equation and analyzed the work of the flow around the cylinder and the atmospheric flow, which is considered to be the beginning of computational fluid dynamics. With the rapid development of computer software and hardware, the Large Eddy Simulation (LES) is generally used in the prediction of turbulent noise due to its faster convergence and higher computational accuracy.[8]

Radavich et al.[9] established the flow and acoustic resonance model at a low Mach number by the CFD and predicted the flow conditions arising from the coupling. Gloerfelt et al.[10] investigated the flow noise problem in a 3D rectangular chamber caused by laminar and turbulent boundary layers using the LES. Larchevêque et al.[11] used the LES to experimentally compare the 3D chamber flow at high Reynolds numbers and the peak frequencies in the simulations were in good agreement with the Rossiter empirical formula. Rubio et al.[12] used the LES to analyze the flow field in a 2D expansion chamber and obtained resonance phenomena inside the chamber and in the tailpipe under the effect of flow noise. The relationship between the vortex modalities in the expansion chamber and the flow velocity and the chamber length was obtained.

In this paper, the study is on low Mach number gas flow at room temperature. The airflow secondary noise in the muffler is considered by the combination of the LES and aeroacoustics theory. Firstly, the LES is used to calculate the unsteady time domain of the flow field in the expansion chamber, then the acoustic analogy method which is in the aeroacoustics theory is used to calculate the noise source in the expansion chamber, and finally, the FEM is used to simulate the acoustic calculation. The article investigates the influence of the relative position of the inlet and outlet pipes on the performance of mufflers, analyzes the generation mechanism of secondary noise in the muffler, and then puts forward the method of suppressing secondary noise by changing the geometric configuration. Finally, the exhaust muffler matched with a dry vacuum pump is modified, and the effectiveness of the suppression structure of secondary noise is verified by both an acoustic simulation and a field test.

2. BASIC THEORY

When there is airflow inside the muffler, the acoustic characteristics of the chamber will change, and the chamber will be transformed from a muffler to a "sounder" due to the vortex of airflow.[13] Muffler secondary noise, also known as regenerative noise, is an additional noise generated in the muffler due to the flow of the medium, which is different from the equipment noise in the pipe. In this paper, the influence of structural changes on the performance of mufflers is analyzed and calculated by combining the LES and aeroacoustics theory.

2.1. Large Eddy Simulation Theory

The LES is a type of emerging algorithm whose computational accuracy is somewhere between the Direct Numerical Simulation method and the Reynolds Average method. The LES adopts the concept of spatial filtering, using the filtering equations to process the Navier-Stokes equations in an unsteady flow field to compute the 3D unsteady flow field. After filtering, the flow field vortices can be divided into two parts: the large and the small scale. The vortices whose scales are smaller than the filtering bandwidth can be filtered out, and only the flow field information of large-scale vortices can be solved directly, which greatly reduces the computational effort while ensuring accuracy.[14]

The filter function equation in the LES is expressed as Eq. (1)[15]

$$G(x,x') = \begin{cases} 1/V, & x' \in V; \\ 0, & x' \notin V; \end{cases} \tag{1}$$

where x is the spatial coordinate on the large-scale space after filtering, x' is the spatial coordinate in the actual flow region and V denotes the size of the geometric space occupied by the control volume.

The Navier-Stokes equation and the continuity equation under an unsteady flow field are treated with the filter equation, which leads to Eqs. (2) and (3)

$$\frac{\partial}{\partial t}\left(\rho\overline{u}_i\right) + \frac{\partial}{\partial x_j}\left(\rho\overline{u}_i\overline{u}_j\right) = \frac{\partial}{\partial x_j}\left(\mu\frac{\partial\overline{u}_i}{\partial x_j}\right) - \frac{\partial\overline{p}}{\partial\overline{x}_i} - \frac{\partial\tau_{ij}}{\partial x_j}; \tag{2}$$

$$\frac{\partial\rho}{\partial t} + \frac{\partial}{\partial x_i}\left(\rho\overline{u}_i\right) = 0. \tag{3}$$

Parameters with the horizontal line above are the quantities of the filtered flow field; u_i and u_j are the velocity components; ρ is the fluid density; μ is the fluid viscosity; and τ_{ij} represents the subgrid-scale stress (SGS), which is a physical quantity characterizing the effect of small-scale vortices within the flow field on the entire flow field and can be expressed as Eq. (4)

$$\tau_{ij} = \rho\overline{u_i u_j} - \rho\overline{u}_i\overline{u}_j. \tag{4}$$

Since the subgrid-scale stress is an unknown parameter, it is required to construct a subgrid-scale model in the process of solving. The WALE (The Wall-Adapting Local Eddy Viscosity Model) model is chosen to construct the subgrid-scale model to solve the small-scale vortices in the unsteady flow field, and the control equations are shown in Eq. (5)[16]

$$\tau_{ij} = \frac{1}{3}\tau_{kk}\delta_{ij} - 2v_t\overline{S}_{ij}; \tag{5}$$

where δ_{ij} is the Kronecker function; $\overline{S}_{ij}$ denotes the deformation rate tensor of the solvable scale and v_t is the subgrid vortex viscosity, represented by Eqs. (6) and (7) respectively

$$\overline{S}_{ij} = \frac{1}{2}\left(\frac{\partial\overline{u}_i}{\partial x_j} + \frac{\partial\overline{u}_j}{\partial x_i}\right); \tag{6}$$

$$v_t = \left(C_s\Delta\right)^2 |\overline{S}|; \tag{7}$$

where C_s is the Smagorinsky constant; Δ is the filter scale; $|\overline{S}|$ is the magnitude of the deformation rate tensor, calculated as

$$|\overline{S}| = \sqrt{2\overline{S}_{ij}\overline{S}_{ij}}. \tag{8}$$

2.2. Aeroacoustics Theory

Lighthill first put forward the acoustic analogy theory, which greatly promoted the development of aeroacoustics. Lighthill proved that the unsteady flow region in an unbounded fluid medium is acoustically equivalent to a quadrupole sound source. Based on Lighthill's research, Curle deduced the formula of aerodynamic noise caused by the interaction between airflow and solid boundary. Curle confirmed that in addition to the quadrupole sound source, the pulsating stress caused by the solid wall boundary can also produce dipole sound radiation. Among the objects studied in this paper, the static solid boundary also has an impact on the sound field, so Curle's theory is used to solve it.[17]

The acoustic analogy theory control equation is shown in Eq. (9)

$$\frac{\partial^2\rho'}{\partial t^2} - c^2\nabla^2\rho' = \frac{\partial^2 T_{ij}}{\partial x_i\partial x_j}; \tag{9}$$

where c is the speed of sound; T_{ij} is the Lighthill stress tensor, which is expressed in Eq. (10)

$$T_{ij} = \rho v_i v_j + p_{ij} - c^2\rho'\delta_{ij}; \tag{10}$$

where ρ' is the density fluctuation and δ_{ij} is the Kronecker function.

The solution to Eq. (9) when considering the effect of solid boundaries is

$$\rho'(x,t) = \frac{1}{4\pi c^2}\left[\frac{\partial^2}{\partial x_i\partial x_j}\int_V \frac{T_{ij}}{|x-y|}\,dV(y) - \frac{\partial}{\partial x_i}\int_S \frac{n_j(\rho v_i v_j + p_{ij})}{|x-y|}\,dS(y)\right]; \tag{11}$$

where x and y denote the location of the observation point and the sound source, respectively; n_j denotes the normal vector perpendicular to the solid boundary surface S. The first term on the right-hand side of the equation represents the quadrupole source caused by fluid motion, and the second term represents the dipole source formed by the solid surface acting on the fluid.

2.3. Performance Evaluation Methods for the Muffler

There are two main criteria for evaluating the acoustic performance of mufflers: transmission loss (TL) and insertion loss (IL). TL is a unique property of the muffler, independent of the piping system and the noise source, and is defined as the difference between the inlet sound power level and the outlet sounds power level of the muffler, expressed as Eq. (12). IL is not only related to the muffler but also reflects the change in the acoustic performance of the whole system (including the muffler, pipe, and noise source) before and after the installation of the muffler, rather than just the muffling performance of the muffler itself. It is defined as the difference in sound pressure levels at fixed measurement points before and after the installation of the muffler and is expressed in the Eq. (13). In the paper, TL is used to characterize muffler performance in muffler acoustic simulation calculations, and IL is used to characterize muffler performance in field noise tests.

$$TL = 10 \log \left(\frac{W_{\text{in}}}{W_{\text{out}}} \right); \tag{12}$$

where W_{in} is the inlet sound power and W_{out} is the outlet sound power,

$$IL = 20 \log \left(\frac{p_1}{p_2} \right); \tag{13}$$

where p_1 and p_2 denote the sound pressure at a measurement point before and after the installation of the muffler.

In addition, aerodynamic performance is another important indicator for evaluating the performance of a muffler. The pressure drop of the muffler is defined as the pressure loss resulting from the airflow through the muffler, expressed as

$$\Delta P = P_{S1} - P_{S2}; \tag{14}$$

where P_{S1} is the average pressure at the inlet; P_{S2} is the average pressure at the outlet.

3. RESEARCH ON ACOUSTIC CHARACTERISTICS OF THE SINGLE-CHAMBER MUFFLER

3.1. Model Building

A single-chamber muffler is the basic acoustic unit of the muffler and usually consists of an inlet pipe, an outlet pipe, and a chamber. Mufflers with interposed pipes are currently widely used. In this paper, the single-chamber muffler is divided into four types (a), (b), (c), and (d), depending on its inlet and outlet positions. Their structural diagram and sizes are shown in Fig. 1 and Table 1, where the length of both the inlet and outlet pipes extending beyond the shell of the muffler is 20 mm.

As shown in Fig. 1, the inlet and outlet pipes of class a muffler are in a straight line; the inlet and outlet pipes of the class b muffler are parallel and located on both sides of the expansion chamber; the inlet and outlet pipes of the class c muffler are perpendicular to each other; the inlet and outlet pipes of the class d muffler are parallel and located on the same side of the expansion chamber.

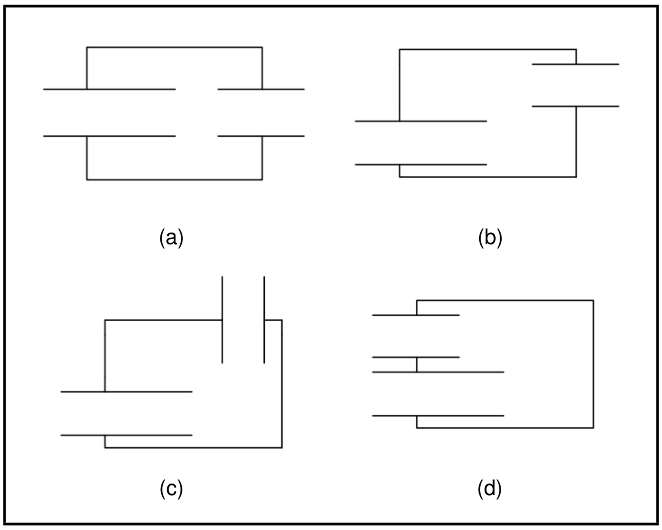

Figure 1. Structure diagrams of different single-chamber mufflers.

Table 1. Structural sizes of single-chamber mufflers.

Parameter	Class a [mm]	Class b [mm]	Class c [mm]	Class d [mm]
Length of inlet pipe	120	120	120	120
Length of outlet pipe	70	70	70	70
Length of chamber	200	200	200	200
Diameter of pipes	40	40	40	40
Diameter of chamber	120	120	120	120

To accurately simulate the unsteady flow field in the expansion chamber, the 3D model of the chamber is established using COMSOL software, and then the grid is divided. A hexahedral structured grid is used in the flow field simulation model to improve computational accuracy and convergence speed. In the near-wall region, sudden expansion and contraction segments increase the grid density to accommodate rapid changes in fluid velocity gradients to reduce calculation errors. The acoustic simulation model does not require a high mesh quality, so the tetrahedral mesh is uniformly used.

As the 3D models of these mufflers are all symmetrical based on longitudinal sections, 1/2 of the 3D model is chosen as the object of study to reduce the computational effort. As shown in Fig. 2, the 3D grid images of each of the four mufflers are shown, where the left-hand side of each row shows the flow field grid and the right-hand side shows the sound field grid. The four muffler models are identical in terms of parameters except for the location of the inlet and outlet pipes.

The unsteady flow field inside the expansion cavity is calculated using the LES in fluid simulation; the unsteady flow process is calculated iteratively using the Pressure Implicit Split Operator (PISO) algorithm. The relevant parameters and boundary conditions for the flow and sound field calculations are shown in Table 2.

3.2. Analysis in the Flow Field

Based on the LES, the flow field analysis of a muffler using COMSOL software requires the setting of parameters such as inlet conditions, outlet conditions, and wall conditions. The initial boundary conditions in this section are set as follows: (1) the airflow velocity expression at the muffler inlet is set to $Ma * c_0$ and the value of c_0 is 343 m/s; (2) the relative pressure at the muffler outlet is set to 0; (3) the inner wall of the

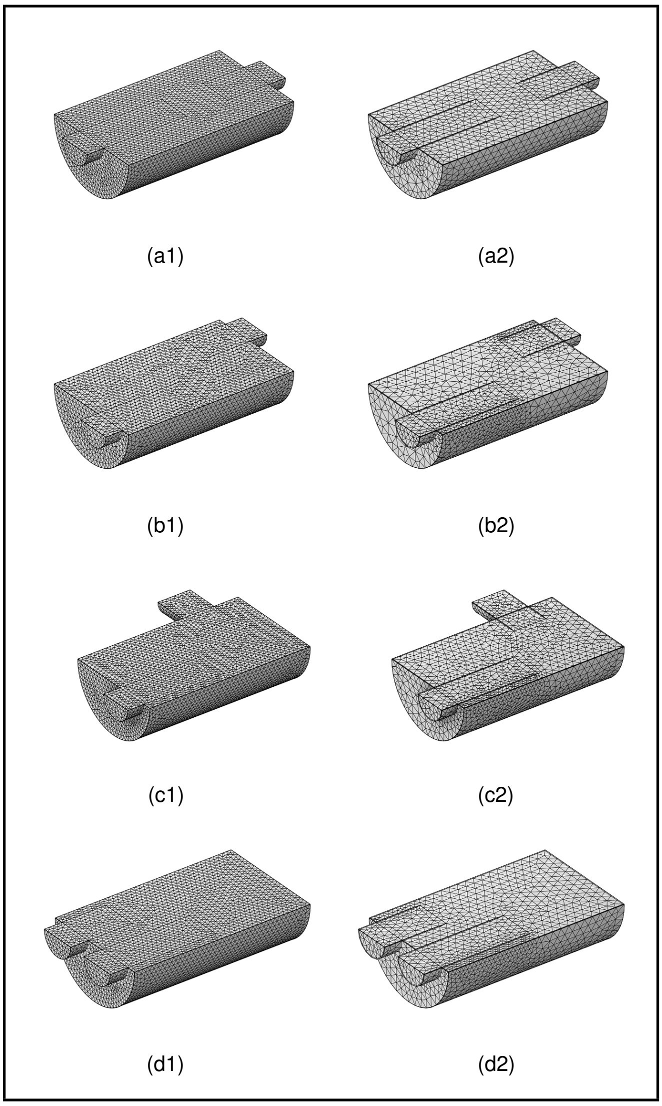

Figure 2. Meshing diagrams of different single-chamber mufflers.

Table 2. Parameters of the simulation.

Parameter	Fluid Simulation	Acoustic Simulation
Grid type	Structured mesh	Tetrahedral mesh
Mesh size	1∼5 mm	3∼9 mm
Step	1/10000 s	10 Hz
Calculation range	0∼0.1 s	20∼2000 Hz
Working media	Air	Air
Inlet condition	Air velocity: 10 m/s	Areflexia
Outlet condition	Pressure: 0 Pa	Areflexia
Wall condition	Rigid, adiabatic and non-slip	Rigid

expansion chamber is set to be a non-slip adiabatic boundary; (4) the longitudinal section of the muffler is set to be a symmetric boundary. The airflow velocity at the inlet is set to be 10.3 m/s ($Ma = 0.03$), and the unsteady flow in the expansion chamber is simulated in the time domain. The flow velocity clouds of the time domain simulation are shown in Fig. 3, and the time shown in the figure are all 0.0111 s.

In Fig. 3, it can be seen that the incident airflow in all four diagrams is injected into the chamber via the inlet of the muffler and a strong shear layer is formed between the incident airflow and the airflow inside the chamber. Most of the incident airflow in figure (a) flows directly into the outlet pipe in the direction of injection, while the flow velocity of the others in the chamber hardly fluctuates, and there is a maximum velocity gradient between the incident airflow and the airflow in the chamber. The incident airflow in figures (b), (c), and (d) impacts the wall in the forward direction of the airflow after entering the chamber and breaks up into vortices of different sizes in the chamber first. The airflow is then disintegrated into a series of vortices of different sizes and then flows out through the outlet through a series of complex flow processes in the chamber.

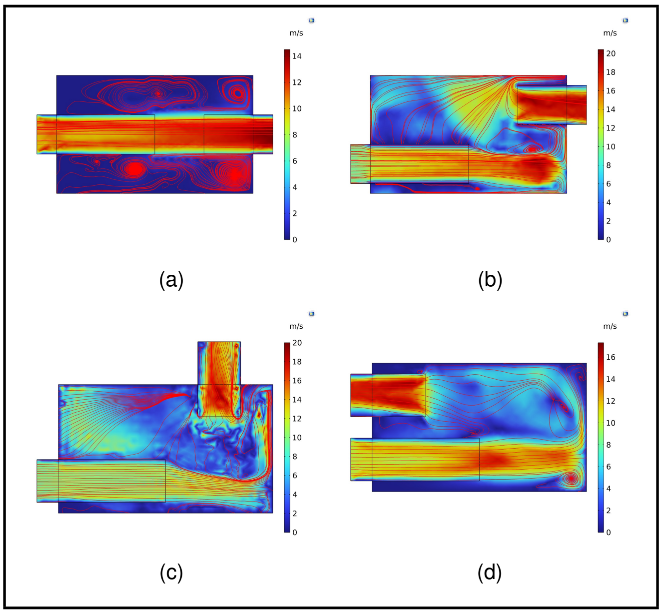

Figure 3. Cloud charts of the velocity in different single-chamber mufflers.

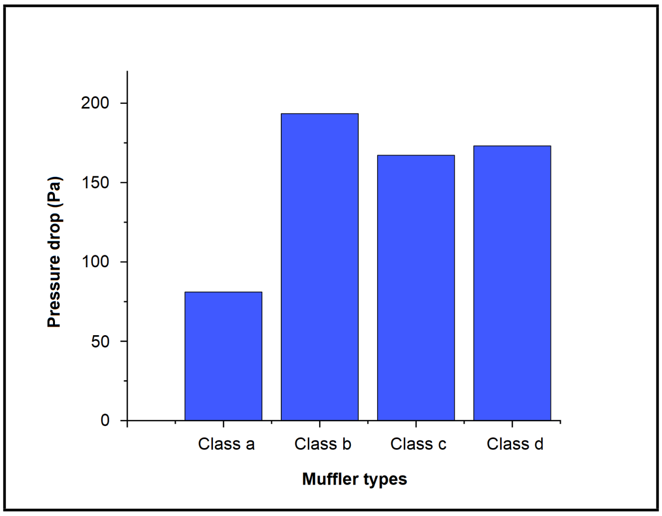

Figure 4. The pressure drop of single-chamber mufflers.

Aerodynamic performance is another important factor that should be considered in the design of a muffler. According to Eq. (14), when the inlet airflow velocity is 10.3 m/s, the average static pressure difference between the inlet and outlet of the muffler is calculated and the results are shown in Fig. 4.

A comparison of the pressure losses of single chamber mufflers of different construction under the same airflow velocity conditions is shown in Fig. 4. From the specific data, it can be seen that the pressure losses of class-b, class-c, and class-d mufflers are relatively close to each other and are all significantly higher than the pressure losses of class-a mufflers. This conclusion is supported by the conclusions drawn in Fig. 3.

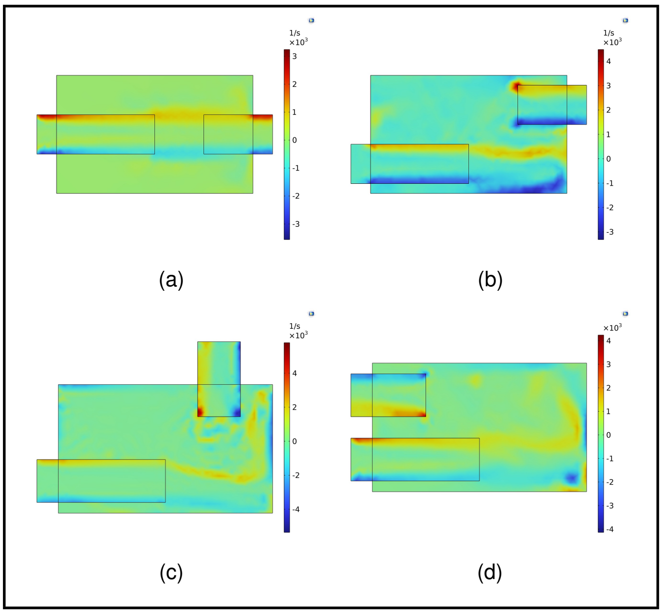

Figure 5. Cloud charts of the vorticity in different single-chamber mufflers.

Vorticity is one of the most important physical quantities to describe vortex motion. It is defined as the curl of the fluid velocity vector and is usually used to describe the non-constant flow process in the flow field. The vortex cloud inside the chamber can be calculated from the previously obtained flow velocity distribution in 3D space. The vortex cloud on the x-y section of the muffler at the time of 0.0111 s is shown in Fig. 5.

Takashi[18] obtained visual images of the airflow in the expansion chamber of a muffler by using the smoke wire technique. Although there are differences in size between the class-a muffler and the muffler used in Takashi's experiments, the structures are similar and the locations of the vortices in the expansion chamber are all essentially the same. Both the simulation results and the vortices observed in Takashi's experiment are concentrated in the middle section of the chamber, which validates the simulation results.

Comparing Fig. 5 and Fig. 3, it can be seen that changing the inlet and outlet positions of the muffler can indeed change the flow pattern of the air in the chamber, which in turn changes the airflow velocity and vortex distribution in the chamber. This provides the basis for the next step to reveal the generation mechanism of the airflow secondary noise in the muffler.

3.3. Analysis in the Sound Field

In the traditional plane wave theory, the transmission loss of the muffler is only related to the cross-sectional area and length of the inlet and outlet pipe and cavity, but not to the positions of the inlet and outlet pipes. In this section, the effect of the positions of the muffler inlet and outlet on its acoustic performance is investigated.[19]

The initial boundary conditions for the analysis of the muffler acoustic performance using COMSOL software are set as follows: (1) the airflow velocity expression of the muffler inlet is set to $Ma * c_0$; (2) the type of inlet pressure acoustic field is set to "plane wave" and the pressure amplitude is set to 1 Pa; (3) the muffler outlet is set to a full sound absorption without reflection boundary; (4) the inner wall of the expansion chamber is set to a non-slip adiabatic boundary; (5) set the longitudinal section of the muffler as a symmetrical boundary; (6) set the frequency domain of the pressure acoustic study to $20 \sim 2000$ Hz with a step size of 20 Hz. Acoustic simulation is carried out under the condition of no flow ($Ma = 0$). The sound power at the inlet and outlet of the muffler are extracted respectively, and then calculated according to Eq. (12) to obtain the transmission loss curves of four types of single-chamber mufflers under no-flow conditions, as shown in Fig. 6 below.

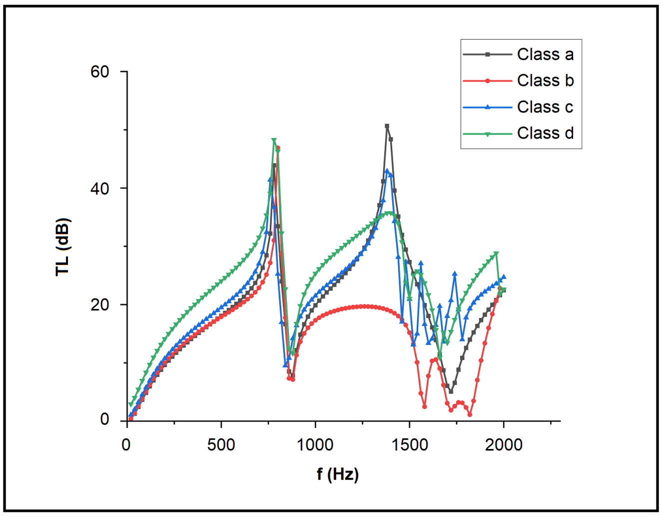

Figure 6. Transmission loss curves of different mufflers in ideal conditions.

As shown in Fig. 6, the trend of the four transmission loss curves is consistent. Among them, the four curves are coincident within the range of 1000 Hz. Beyond 1000 Hz, the transmission loss curve of the class b muffler is clearly at the lowest. Although there are differences in individual frequency bands, the transmission loss curves of the remaining three mufflers can still be regarded as approximate. The average transmission losses of the four single-chamber mufflers are 19.59 dB, 14.69 dB, 20.59 dB, and 23.92 dB in order. This is consistent with the conclusion drawn from conventional plane wave theory and also indirectly proves the reliability of the simulation results.

After calculating the internal flow field of the expansion chamber using the LES, the Lighthill theory is applied to the calculation of the flow noise source. The flow field information such as velocity, temperature, pressure, and density are extracted by the integral interpolation method and mapped to the acoustic grid. The flow noise source is then solved on the acoustic grid according to the aeroacoustic theory, and the Fourier transform is carried out to obtain the results in the frequency domain. The flow noise cloud with a frequency of 1300 Hz is shown in Fig. 7.

It is clear from Fig. 7 that the airflow noise sources in the expansion chamber are mainly distributed in the locations where the swirls in the chamber are concentrated, i.e., where there is a large velocity gradient and where the airflow hits the wall. Comparing Fig. 7 with Fig. 3, it can be found that the distribution of noise sources is closely related to the fluctuation of the flow velocity in the expansion chamber, and the larger the velocity gradient, the more likely it is to generate secondary noise.

A monitoring point is established at the muffler outlet and

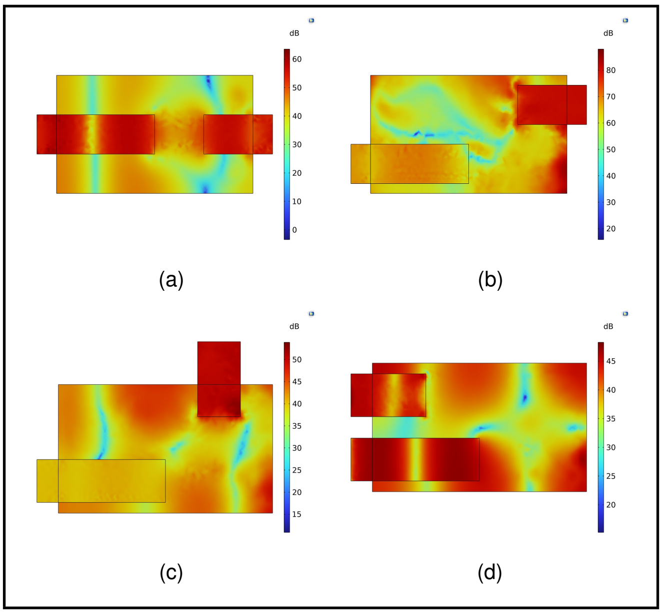

Figure 7. Cloud charts of the sound field distribution in different single-chamber mufflers.

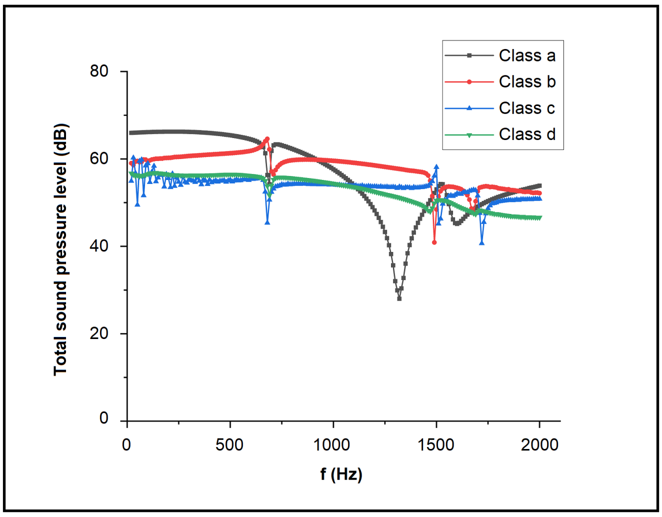

Figure 8. Sound pressure level curves at the outlet of different mufflers.

the sound pressure value at this point is calculated and extracted. In Fig. 8, the sound pressure levels at the outlet of the four mufflers are compared.

The physical quantities such as mean flow velocity, pressure, and turbulent viscosity obtained from the fluid simulation are used as background parameters. Setting Ma in the airflow velocity expression to 0, 0.03, 0.05, and 0.1 in order, the transmission loss curves of different single-chamber mufflers at different flow conditions are calculated according to Eq. (12) respectively, as shown in Fig. 9.

The transmission loss curves for the four types of single-chamber mufflers at the same airflow conditions when the inlet air flow rate is 10 m/s, as shown in Fig. 10.

The following conclusions can be drawn from the analysis of the above several figures: (1) In Fig. 8, the average sound pressure levels at the outlet of the four types of single-chamber mufflers, (a), (b), (c), and (d), are 56.32 dB, 57.73 dB, 53.43 dB, and 52.85 dB. The airflow secondary noise of the class-d muffler is the smallest, and the transmission loss is the least affected by the change of the airflow speed; (2) In Fig. 9, the transmission loss of all mufflers is reduced by the influence of the secondary noise of airflow, and the greater the airflow speed, the greater the reduction; (3) In Fig. 10, mufflers of different structures are affected differently. Under the same flow conditions, the amplitude of the transmission loss curve of the class-b muffler is lower than that of other types, and its noise reduction ability is the worst; (4) In Fig. 10, the amplitude of the transmission loss curve of the class-d muffler is the highest, and the average transmission losses of the four types of single-chamber mufflers, (a), (b), (c), and (d), are 17.45 dB, 8.09 dB, 18.52 dB, and 22.01 dB respectively. In summary, under low Mach number flow conditions, the inlet and outlet position of the muffler has a great influence on its noise reduction ability. The acoustic performance of class-d muffler is optimal, and this structure should be preferred in the design of mufflers.

Table 3. Structural sizes of mufflers.

Parameter	Muffler-A [mm]	Muffler-B [mm]
Length of inlet pipe	63	169
Length of outlet pipe	46	132
Length of intermediate pipe	75	79
Diameter of pipes	20	20
Lengths of each chamber	86–106	106–86
Diameter of chambers	102	102

4. SUPPRESSION METHOD OF THE AIRFLOW SECONDARY NOISE

4.1. Simulation Analysis

A certain type of dry vacuum pump has a matching double-chamber exhaust muffler. Based on the conclusions drawn in Section 3, the structure is modified while keeping the overall dimensions of the muffler unchanged. The two single-chamber mufflers of class a, which are connected in series, are replaced by two single-chamber mufflers of class d, which are combined. The improved muffler ensures that the inlet and outlet directions remain unchanged. The 3D model and main parameters of mufflers are shown in Fig. 11 and Table 3.

According to the method in Section 3, the LES and the flow noise source calculations are carried out for the muffler in Fig. 11 when the inlet airflow velocity is 10 m/s. The flow velocity cloud, the vortex cloud, and the flow noise cloud inside different mufflers are obtained as shown in Fig. 12.

It can be shown in Fig. 12 that the flow velocity distribution, vortex distribution, and flow noise source distribution inside the muffler have all changed significantly after the internal structure has been changed. The sound pressure values of the observation points at the outlet are calculated and extracted separately to obtain the sound pressure level curves at the muffler outlet, as shown in Fig. 13.

The pressure field type of the inlet of the muffler is set to "plane wave", the pressure amplitude is set to 1 Pa, and the outlet of the muffler is a full sound absorption without reflection boundary. When the inlet airflow velocity is 10 m/s, the transmission losses of the two types of double-chamber mufflers are calculated with and without considering the airflow secondary noise, as shown in Fig. 14.

In Fig. 14, the transmission losses are reduced for both muffler-A and muffler-B when considering the airflow sec-

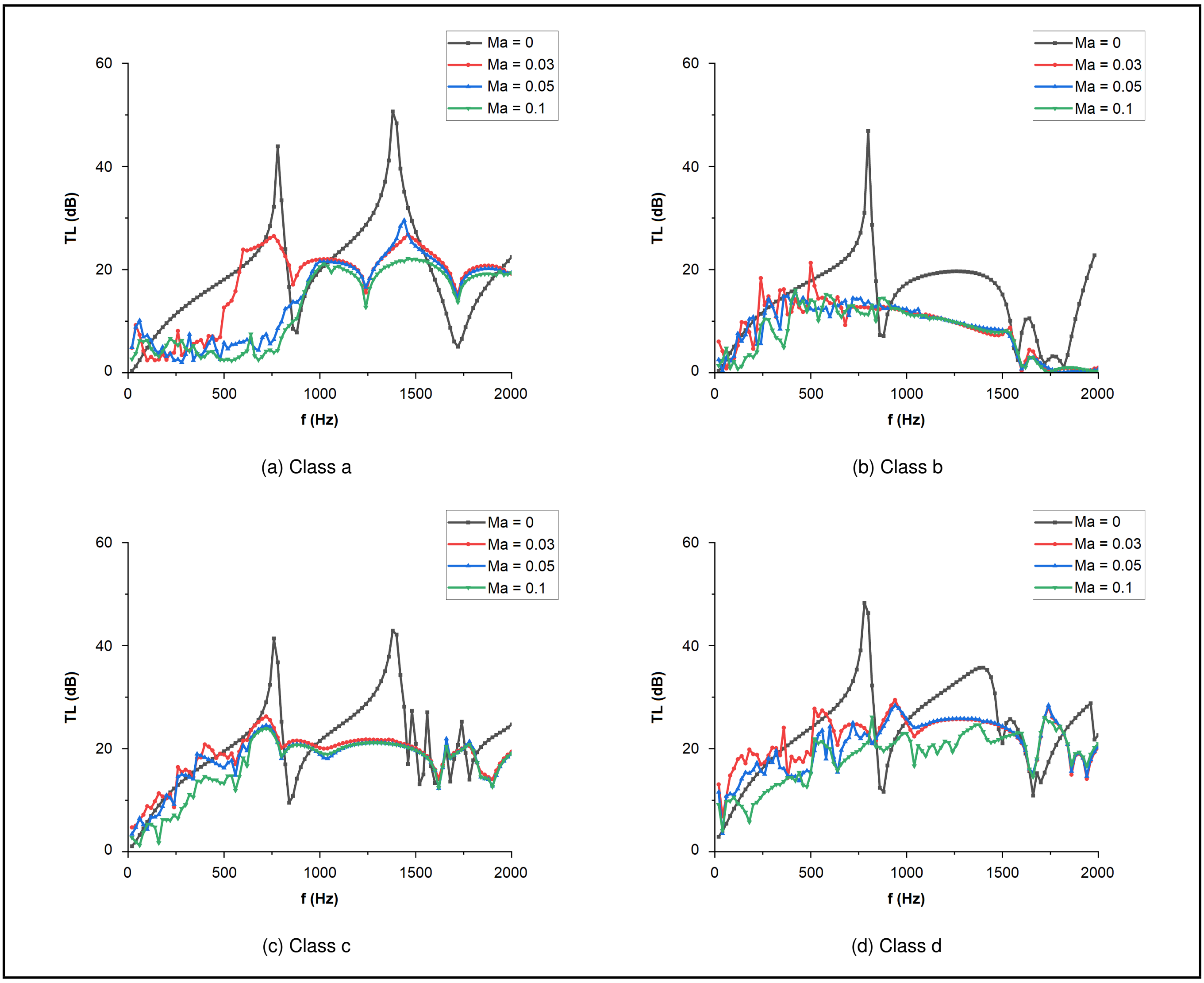

Figure 9. Transmission loss curves of mufflers with and without flow conditions.

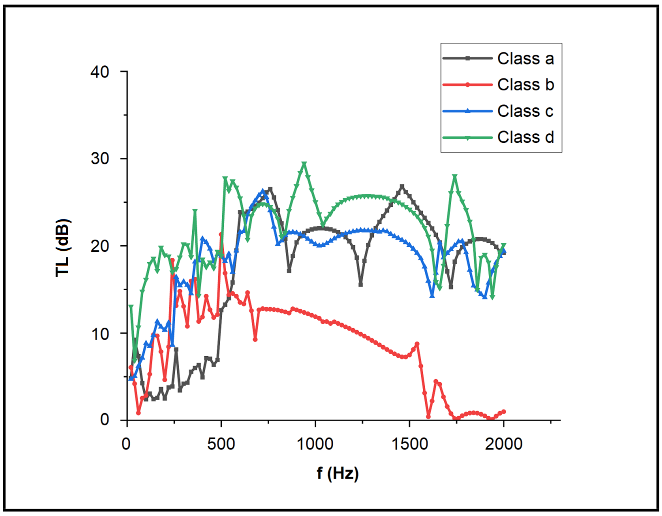

Figure 10. Transmission loss curves of different single-chamber mufflers.

ondary noise, with the average transmission loss over the full frequency range reduced by 3.41 dB (about 8.5%) for muffler-A and by 1.97 dB (about 4.5%) for muffler-B.

The transmission loss curves of muffler-A and muffler-B are compared for the same airflow conditions, as shown in Fig. 15.

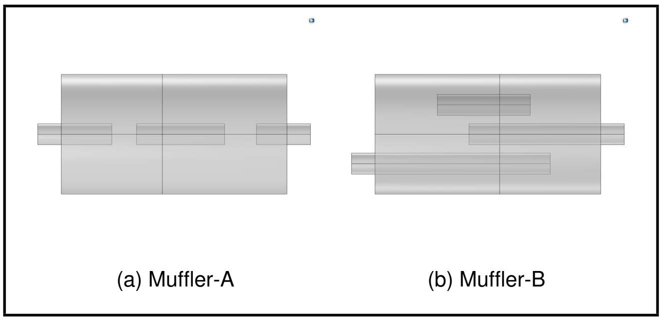

Figure 11. Structure diagrams of mufflers.

The following conclusions can be drawn from the analysis of Figs. 13, 14, and 15: (1) the airflow secondary noise intensity of muffler-B is lower than that of muffler-A; (2) the amplitude of the transmission loss curve of muffler B in the middle and low-frequency range (100 $\sim$ 1500 Hz) is substantially higher than that of muffler-A, while the two transmission loss curves in the other frequency ranges are close to each other. In the whole frequency range, the transmission losses of muffler-A and muffler-B are 36.4 dB and 43.2 dB respectively, with a difference of 6.8 dB. In summary, the structure of the class d single-chamber muffler can reduce the intensity of the airflow

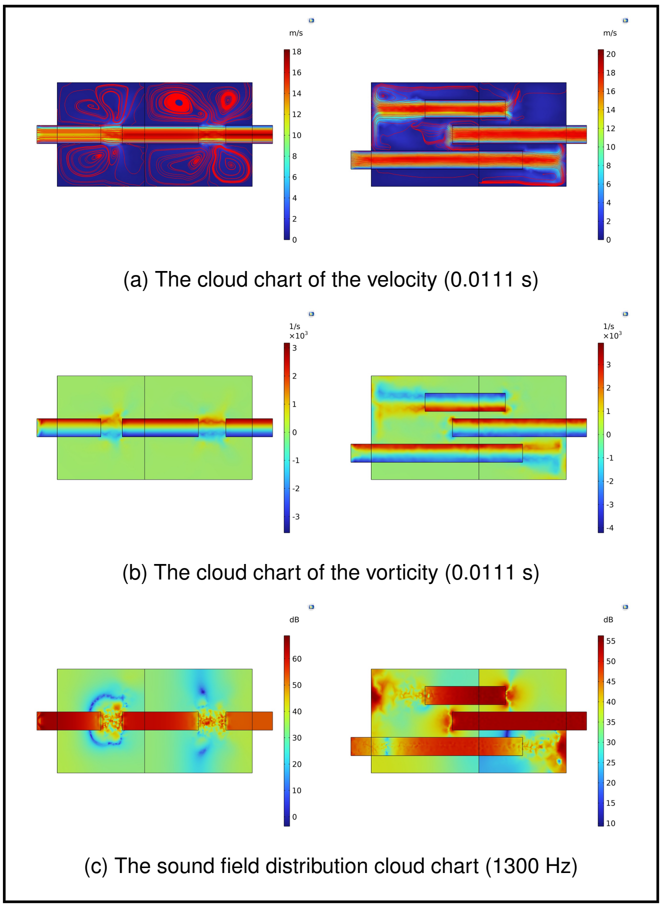
(a) The cloud chart of the velocity (0.0111 s)
(b) The cloud chart of the vorticity (0.0111 s)
(c) The sound field distribution cloud chart (1300 Hz)

Figure 12. Comparison of simulation results of different mufflers.

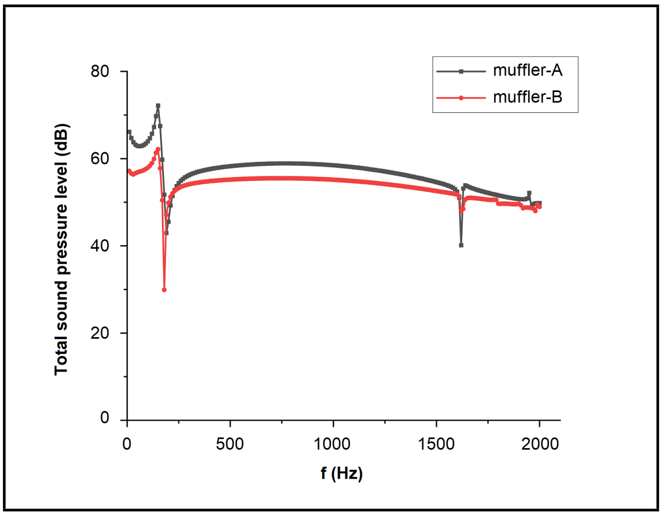

Figure 13. The sound pressure level curves at the muffler outlet.

secondary noise, and muffler-B has a significant improvement over muffler-A in terms of noise reduction capability.

4.2. Sample Testing

According to the test specification ISO 11820:1996, an open room of 200 m^2 in a factory was selected as the test room. The dry vacuum pump used for the test was in steady operation with an exhaust volume of 14.4 m^3/h. Samples of muffler-A and muffler-B in Fig. 11 were made as test objects and the other main test instruments are shown in Table 4. The measurement points were arranged in the center of the room, using a

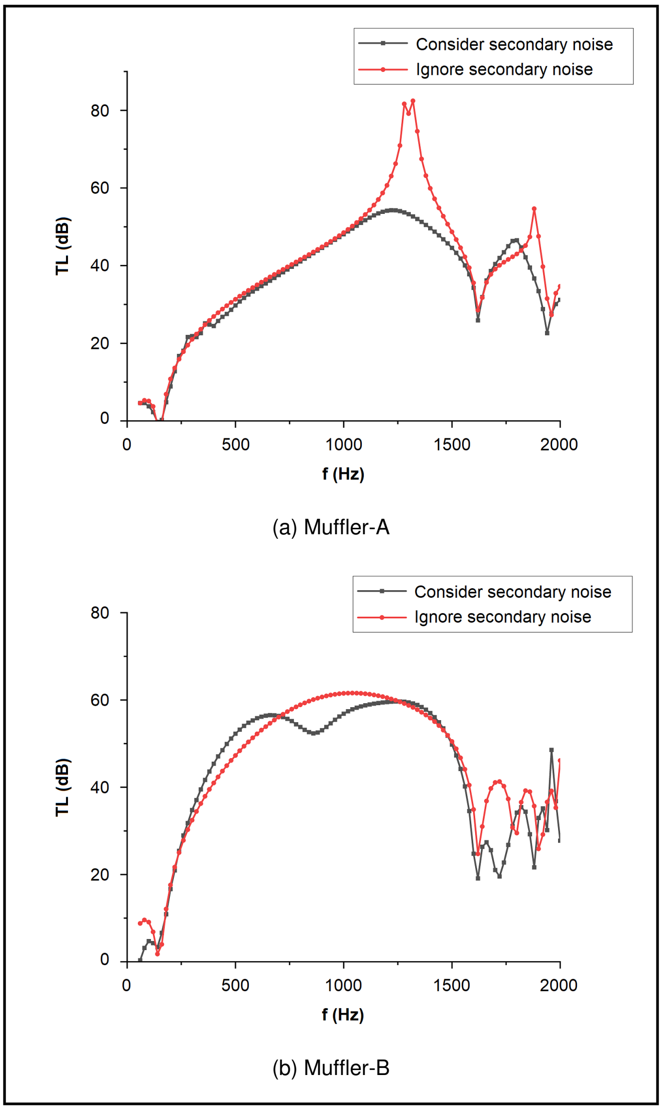

(a) Muffler-A
(b) Muffler-B

Figure 14. Transmission loss curves of the muffler.

Table 4. List of the main equipment for noise tests.

Equipment name	Category	Number
Data acquisition analyzer	3560-D	1
B&K data acquisition and analysis software	Pulse v12.5	1
Microphone	G.R.A.S. 26CA	1
Notebook computer	Dell	1

bracket to place the microphone above the muffler exhaust port at 45 degrees, more than 1 m from the exhaust port. To ensure that the sound waves are in the same direction of incidence, the position of the measurement points should remain constant during the noise measurement, and the test site is shown in Fig. 16.[20]

Samples of the two mufflers from Fig. 11 were manufactured and fitted to the matching dry vacuum pump for noise testing, as shown in Fig. 17.

The noise test is carried out according to the previous method and the noise octave spectrums of the mufflers are obtained, as shown in Fig. 18.

The noise test data in Fig. 18 is compared and analyzed. It is found that the vacuum pump equipped with the muffler-B shows a reduction in noise values in all frequency bands compared to the muffler-A, with the improvement being particularly noticeable in the low and medium frequency bands. This

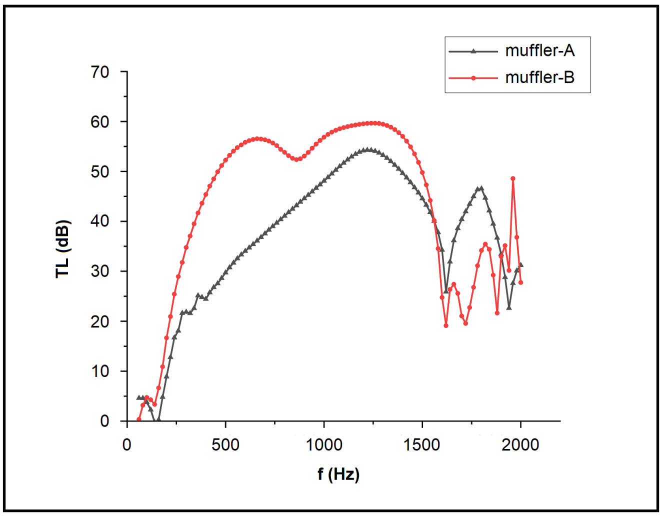

Figure 15. Comparison of transmission loss curves of mufflers.

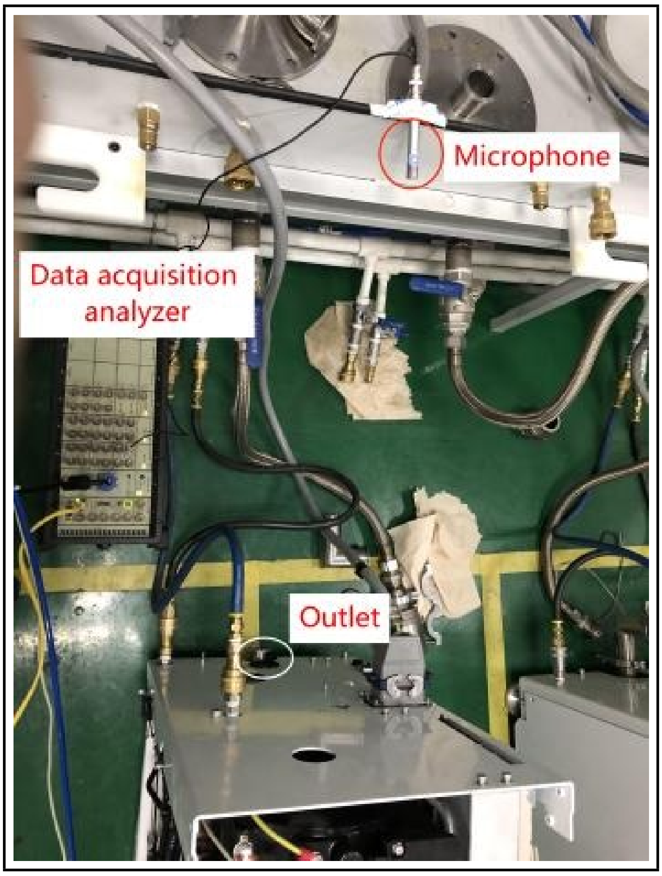

Figure 16. The picture of the noise test site.

phenomenon is consistent with the conclusions drawn from the simulation in Fig. 15. The noise reduction of the two mufflers obtained from the field test is 31.9 dB and 37.6 dB, respectively, an improvement of 5.7 dB (about 18%). Therefore, it can be concluded that the choice of class d single-chamber muffler structure in the muffler design can improve the noise reduction capacity of the muffler.

5. CONCLUSIONS

Based on previous studies, this paper further considers the effect of the secondary noise on the airflow of the muffler, and

Figure 17. The picture of the muffler sample.

the goal is to improve its acoustic performance. Taking the single-chamber muffler as the research object, the paper investigates the acoustic performance of the muffler under the consideration of acoustic-flow coupling, analyzes the influence of different structures on the airflow secondary noise of the muffler, and finally modifies a double-chamber muffler according to the conclusions. The conclusions of the present paper include the following.

(1) The paper used LES and the acoustic analogy analysis method to calculate the unsteady flow of air and airflow secondary noise in four types of single-chamber mufflers. The LES was used to calculate the unsteady airflow inside the muffler, and the simulation results visualized the unsteady eddy formation process caused by the velocity gradient of the airflow inside the chamber. The main source of the airflow secondary noise in the muffler was the formation and shedding of the vortex inside the expansion chamber. The airflow entered the expansion chamber through the muffler inlet and created a vortex structure under the action of viscous forces. The vortex gradually increased in size as the airflow was pushed downstream and then fell off.

(2) The effect of flow velocity on the airflow secondary noise was significant and the greater the airflow velocity, the greater the effect of the secondary noise on the performance of the muffler. Under the same airflow conditions, mufflers of different structures have different suppression effects on the airflow secondary noise. In this paper, the single-chamber muffler was divided into four structures

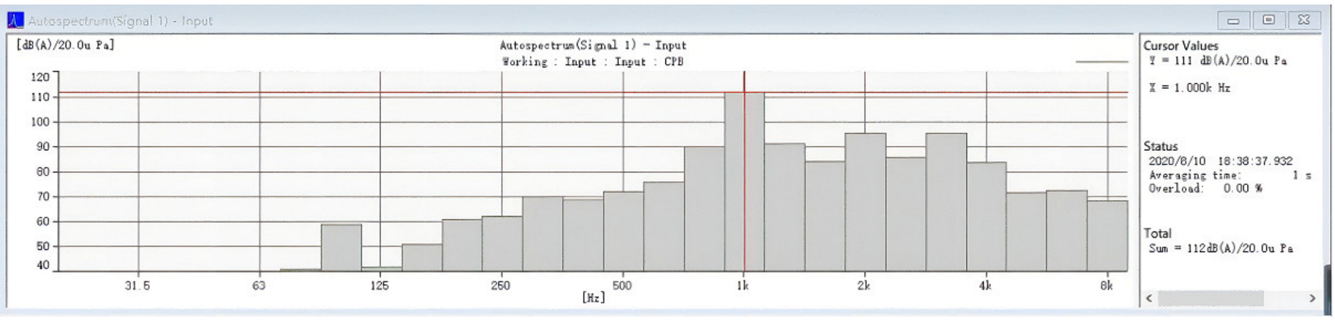

(a) Noise spectrum of a vacuum pump without a muffler

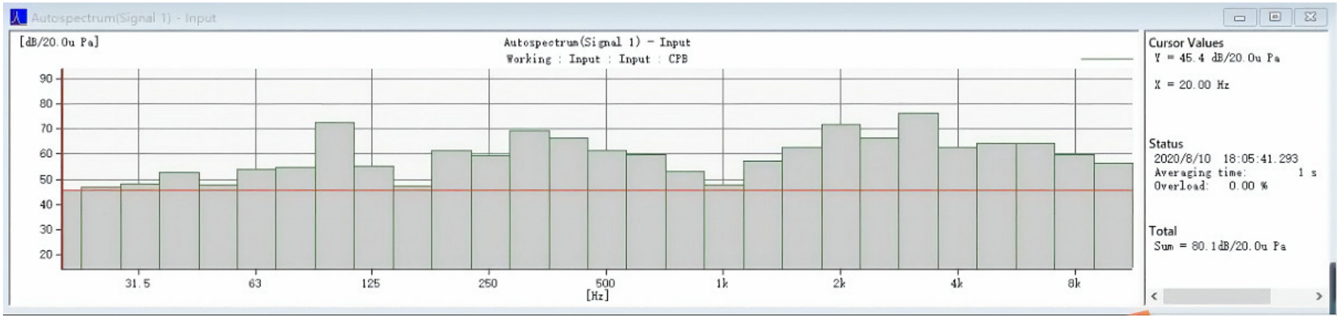

(b) Noise spectrum of a vacuum pump with the muffler-A

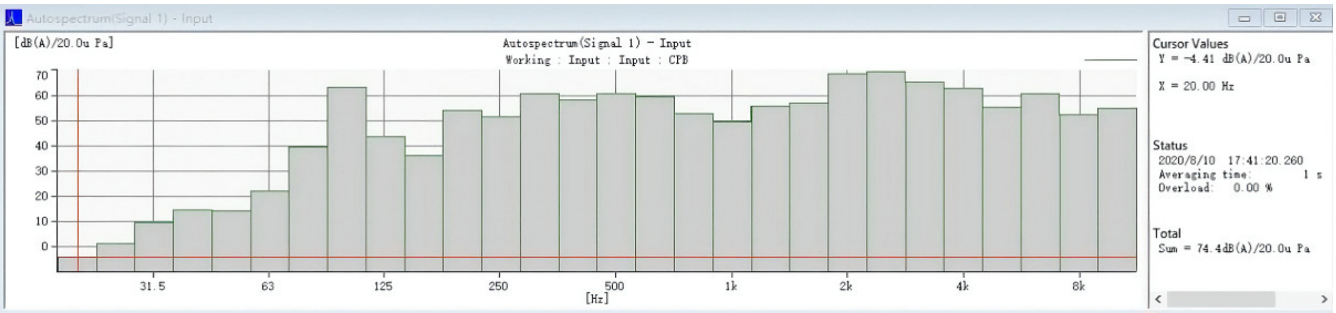

(c) Noise spectrum of a vacuum pump with the muffler-B

Figure 18. The result of the noise test.

according to the relative positions of the inlet and outlet pipes, and the sound source distribution of the airflow secondary noise was calculated by extracting the flow field information, and the sound pressure value of the airflow noise of the observation point at the outlet of the muffler was obtained by combining the acoustic analogy method. The acoustic characteristics of the four types of mufflers were analyzed, and it was found that the use of the class-d single-chamber muffler structure can result in a muffler with better and more stable muffling capacity.

(3) The conclusions obtained in the single chamber muffler were extended to the double chamber muffler and the structure of a double-chamber exhaust muffler was modified by replacing the connecting structure with the structure of the class-d single-chamber muffler. Acoustic simulations and field noise tests demonstrate that the performance of the improved muffler was improved. It was shown that by changing the position of the muffler inlet and outlet, the airflow in the muffler can be changed, suppressing the formation of vortices in the chamber, and significantly reducing the intensity of the airflow secondary noise. The research in this paper has a certain significance in reducing the secondary noise of the airflow and improving the muffler performance of the exhaust muffler.

REFERENCES

[1] Gupta, A., Gupta, A., Jain, K., and Gupta, S. Noise pollution and impact on children health, *The Indian Journal of Pediatrics*, **85** (4), 300–306, (2018). https://doi.org/10.1007/s12098-017-2579-7

[2] Huang, H., Chen, Z., and Ji, Z. One-way fluid-to-acoustic coupling approach for acoustic attenuation predictions of perforated silencers with non-uniform flow, *Advances in Mechanical Engineering*, **11** (5), (2019). https://doi.org/10.1177/1687814019847066

[3] Rehman, H., Chung, H., Joung, T., Suwono, A., and Jeong, H. CFD analysis of sound pressure in tank gun muzzle silencer, *Journal of Central South University of Technology*,

18 (6), 2015–2020, (2011). https://doi.org/10.1007/s11771-011-0936-7

4 Xiang, L., Zuo, S., Wu, X., and Liu, J. Study of multi-chamber micro-perforated muffler with adjustable transmission loss, *Applied Acoustics*, **122**, 35–40, (2017). https://doi.org/10.1016/j.apacoust.2017.01.034

5 Moin, P. Advances in large eddy simulation methodology for complex flows, *International Journal of Heat and Fluid Flow*, **23** (5), 710–720, (2002). https://doi.org/10.1016/s0142-727x(02)00167-4

6 Ji, Z. L. and Selamet, A. Boundary element analysis of three-pass perforated duct mufflers, *Noise Control Engineering Journal*, **48** (5), 151, (2000). https://doi.org/10.3397/1.2827962

7 Liu, L., Qiu, Y., Hao, Z., and Zheng, X. A modified time domain approach for calculation of noise reduction and acoustic impedance of intake duct system, *Applied Acoustics*, **168**, 107420, (2020). https://doi.org/10.1016/j.apacoust.2020.107420

8 Piomelli, U., Streett, C. L., and Sarkar, S. On the computation of sound by large-eddy simulations, *Journal of Engineering Mathematics*, **32** (2), 217–236, (1997). https://doi.org/10.1023/A:1004236206327

9 Radavich, P. M., Selamet, A., and Novak, J. M. A computational approach for flow-acoustic coupling in deep cavities, *Journal of the Acoustical Society of America*, **108** (5), 2451–2451, (2000). https://doi.org/10.1121/1.4743029

10 Gloerfelt, X., Bogey, C., Bailly, C., and Juve, D. Aerodynamic noise induced by laminar and turbulent boundary layers over rectangular cavities, *8th AIAA/CEAS Aeroacoustics Conference and Exhibit*, (2002). https://doi.org/10.2514/6.2002-2476

11 Larchevêque, L., Sagaut, P., Lê, T.-H., and Comte, P. Large-eddy simulation of a compressible flow in a three-dimensional open cavity at high Reynolds number, *Journal of Fluid Mechanics*, **516**, 265–301, (2004). https://doi.org/10.1017/s0022112004000709

12 Rubio, G., De Roeck, W., Desmet, W., and Baelmans, M. Large eddy simulation for computation of aeroacoustic sources in 2D-expansion chambers, in *Direct and Large-Eddy Simulation VI*, Lamballais, E., et al. (Eds), Springer, Dordrecht, 555–564, (2006). https://doi.org/10.1007/978-1-4020-5152-2_64

13 English, E. J., Holland K. R. Aeroacoustic sound generation in simple expansion chambers, *Journal of the Acoustical Society of America*, **128** (5),2589–2595, (2010). https://doi.org/10.1121/1.3483735

14 Moin, P. Advances in large eddy simulation methodology for complex flows, *International Journal of Heat and Fluid Flow*, **23** (5), 710–720, (2002). https://doi.org/10.1016/s0142-727x(02)00167-4

15 Wagner, E. and Hüttl, T. *Large-Eddy Simulation for Acoustics*, Cambridge University Press, (2007). https://doi.org/10.1017/CBO9780511546143

16 Nana, C., Marx, D., Prax, C., and Fortuné, V. Hybrid aeroacoustic computation of a low Mach number non-isothermal shear layer, *Computers and Fluids*, **93**, 30–40, (2014). https://doi.org/10.1016/j.compfluid.2014.01.006

17 Guoqing, H., Dexun, F. U., and MaYanwen Numerical simulation of noise generated by flow past an airfoil using acoustic analogy (in Chinese), *Chinese Journal of Theoretical and Applied Mechanics*, **32** (4), 392–401, (2000). https://doi.org/10.3321/j.issn:0459-1879.2000.04.002

18 Esaki, T., Yokota, S., Mikami, M., and Kojima, N. Characteristics of sound sources of pulsating flow induced noise in a muffler cavity, *The Proceedings of the JSME Annual Meeting*, **2003.7**, 261–262, (2003). https://doi.org/10.1299/jsmemecjo.2003.7.0_261

19 Mohamad, B. A review of flow acoustic effects on a commercial automotive exhaust system—methods and materials, *Journal of Mechanical and Energy Engineering*, **3** (43), 149–156, (2019). https://doi.org/10.30464/jmee.2019.3.2.149

20 ISO 11820: Measurements on silencers in situ, (1996). https://doi.org/10.3403/01149187